



ARTICLE

In vivo proximity proteomics uncovers palmdelphin (PALMD) as a Z-disc-associated mitigator of isoproterenol-induced cardiac injury

Cong-ting Guo¹, Blake D. Jardin², Jun-sen Lin¹, Rachele L. Ambroise³, Ze Wang¹, Lu-zi Yang¹, Neil Mazumdar², Fu-jian Lu^{2,4}, Qing Ma², Yang-po Cao⁵, Can-zhao Liu⁶, Kai-long Li⁷, Xu-jie Liu⁸, Feng Lan⁸, Ming-ming Zhao^{9,10,11}, Han Xiao^{9,10,11}, Er-dan Dong^{9,10,11,12}, William T. Pu²✉ and Yu-xuan Guo^{1,10,11}✉

Z-discs are core ultrastructural organizers of cardiomyocytes that modulate many facets of cardiac pathogenesis. Yet a comprehensive proteomic atlas of Z-disc-associated components remain incomplete. Here, we established an adeno-associated virus (AAV)-delivered, cardiomyocyte-specific, proximity-labeling approach to characterize the Z-disc proteome in vivo. We found palmdelphin (PALMD) as a novel Z-disc-associated protein in both adult murine cardiomyocytes and human pluripotent stem cell-derived cardiomyocytes. Germline and cardiomyocyte-specific *Palmd* knockout mice were grossly normal at baseline but exhibited compromised cardiac hypertrophy and aggravated cardiac injury upon long-term isoproterenol treatment. By contrast, cardiomyocyte-specific PALMD overexpression was sufficient to mitigate isoproterenol-induced cardiac injury. PALMD ablation perturbed the transverse tubule (T-tubule)-sarcoplasmic reticulum (SR) ultrastructures, which formed the Z-disc-associated junctional membrane complex (JMC) essential for calcium handling and cardiac function. These phenotypes were associated with the reduction of nexilin (NEXN), a crucial Z-disc-associated protein that is essential for both Z-disc and JMC structures and functions. PALMD interacted with NEXN and enhanced its protein stability while the *Nexn* mRNA level was not affected. AAV-based NEXN addback rescued the exacerbated cardiac injury in isoproterenol-treated PALMD-depleted mice. Together, this study discovered PALMD as a potential target for myocardial protection and highlighted in vivo proximity proteomics as a powerful approach to nominate novel players regulating cardiac pathogenesis.

Keywords: proximity proteomics; sarcomere Z-disc; isoproterenol induced cardiac injury; palmdelphin

Acta Pharmacologica Sinica (2024) 0:1–13; <https://doi.org/10.1038/s41401-024-01348-y>

INTRODUCTION

Myofibrils are the specialized actomyosin complexes that drive the contraction and relaxation of muscle cells. In cardiomyocytes, the structural and functional units of myofibrils are called sarcomeres, which are interconnected at their boundaries named Z-discs [1, 2]. Z-discs are assembled by α -actinin-2 (ACTN2), which crosslinks antiparallel actin filaments from adjacent sarcomeres, providing anchorage sites for an array of other sarcomere-associated proteins. In addition to the structural role of Z-discs, Z-discs are a hub for signal transduction and gene expression regulation [3, 4].

Z-discs provide the scaffold for other critical subcellular structures, particularly the transverse tubules (TTs) and the

sarcoplasmic reticulum (SR). TTs are tubular, transverse invaginations of plasma membrane that are observed specially in striated muscle cells. TTs facilitate the propagation of action potentials from the cell surface into cell interior to activate the L-type calcium channel $Ca_v1.2$. The SR is a specialized endoplasmic reticulum (ER) that stores calcium and mediates calcium release via the calcium channel ryanodine receptor 2 (RyR2). TT and SR membranes closely associate with each other via junctophilin-2 (JPH2) at subcellular microdomains known as the junctional membrane complexes (JMCs). JMCs closely juxtapose $Ca_v1.2$ on the TT with RyR2 on the SR and facilitate $Ca_v1.2$ -mediated RyR2 activation and calcium release from SR into cytoplasm. This

¹School of Basic Medical Sciences, Institute of Cardiovascular Sciences, Peking University Health Science Center, Beijing 100191, China; ²Department of Cardiology, Boston Children's Hospital, Boston, MA, USA; ³Harvard College, Harvard University, Cambridge, MA, USA; ⁴Institutes of Biomedical Sciences, Fudan University, Shanghai 200032, China; ⁵Department of Pharmacology, Joint Laboratory of Guangdong-Hong Kong Universities for Vascular Homeostasis and Diseases, School of Medicine, Southern University of Science and Technology, Shenzhen 518055, China; ⁶Department of Cardiology, Translational Medicine Research Center, Zhujiang Hospital, Southern Medical University, Guangzhou 510280, China; ⁷Department of Biochemistry and Molecular Biology, Beijing Key Laboratory of Protein Posttranslational Modifications and Cell Function, School of Basic Medical Sciences, Peking University Health Science Center, Beijing 100191, China; ⁸Shenzhen Key Laboratory of Cardiovascular Disease, Fuwai Hospital Chinese Academy of Medical Sciences, Shenzhen 518057, China; ⁹Department of Cardiology and Institute of Vascular Medicine, Peking University Third Hospital, Beijing 100191, China; ¹⁰State Key Laboratory of Vascular Homeostasis and Remodeling, Peking University, Beijing 100191, China; ¹¹Beijing Key Laboratory of Cardiovascular Receptors Research; NHC Key Laboratory of Cardiovascular Molecular Biology and Regulatory Peptides, Beijing 100191, China and ¹²Research Center for Cardiopulmonary Rehabilitation, University of Health and Rehabilitation Sciences Qingdao Hospital (Qingdao Municipal Hospital), School of Health and Life Sciences, University of Health and Rehabilitation Sciences, Qingdao 266071, China

Correspondence: William T Pu (william.pu@cardio.chboston.org) or Yu-xuan Guo (guo@bjmu.edu.cn)

Received: 25 March 2024 Accepted: 28 June 2024

Published online: 23 July 2024

mechanism results in the close coupling of cardiac excitation with sarcomere contractility [5, 6].

JMCs are located at subdomains of TTs proximal to Z-discs, but how Z-discs interplay with JMCs to modulate cardiomyocyte function remains poorly understood. Nexin (NEXN) likely mediates the crosstalk between Z-discs and JMCs. On one hand, NEXN is known as an actin filament-binding protein that maintains Z-disc stability [7]. On the other hand, NEXN associates with JMCs and is required for TT organization [8]. Human mutations in *NEXN* cause inherited cardiomyopathy [7, 9]. Therefore, understanding the regulation and function of NEXN in association with JMCs and Z-discs is necessary to elucidate the mechanisms behind cardiac pathogenesis.

Comprehensive mapping of Z-disc-associated proteins is pivotal to elucidate the molecular mechanisms underlying cardiac pathophysiology. Proximity labeling is recently emerging as a powerful approach to depict the proteomics of the Z-disc and TT/JMC subdomains [10–12]. This technology relies on a promiscuous biotin ligase such as BirA* or BioID2 [13, 14] or an engineered peroxidase such as APEX2 [15] to biotinylate proteins adjacent to a given bait. These biotin-labeled proteins are then purified by streptavidin beads and characterized by mass spectrometry [13, 14].

To date, multiple proximity proteomics analyses have been reported to characterize the Z-disc, TTs or JMCs. These protein baits include $Ca_v1.2$ [16], JPH2 [17], TTN [18], and ACTN2 [19]. One major technical concern in these studies involves the use of an in vitro cell culture system. Both heart-derived [16] and stem-cell differentiated [19] cardiomyocytes in cell culture are known to exhibit immature phenotypes including Z-disc disarray and TT disruption [20, 21]. Thus, whether in vitro proximity proteomics represents Z-disc/TT proteome in native cardiomyocytes remains questionable. Alternatively, transgenic or knock-in mice expressing BirA*, BioID2, or APEX2 have been reported to enable in vivo proximity proteomics in the heart [16–18]. However, in these approaches, the BioID tags could potentially perturb the function of endogenous proteins and disrupt the proximity proteome.

To overcome the above technical issues, we recently harnessed adeno-associated virus (AAV) as the gene delivery vector to perform cardiomyocyte-specific proximity labeling in mice. With the adjustable dosage of AAV, the BioID fusion protein could be controlled at a low level to circumvent potential impact on the endogenous proteins. Using JMC markers Triadin and Junctin as baits, we successfully identified a novel regulator of JMCs [12]. Here, we established a new AAV-based ACTN2-BioID2 vector to perform in vivo proximity proteomics analysis of cardiomyocyte Z-discs in mice. We identified a novel Z-disc-associated protein, palmdelphin (PALMD), that plays a critical role in modulating Z-disc-JMC tethering and cardiac pathogenesis.

MATERIALS AND METHODS

Animal

Animal strains and procedures were approved by the Institutional Animal Care and Use Committee of Boston Children's Hospital (19-07-3969R) and Peking University (LA2021332). The *Rosa^{Cas9-Tom}* mice were purchased from GemPharmatech (Strain No. T002249) and validated as previously described [22]. The *Palmd^{-/-}* mice were generated at Mouse Gene Manipulation Core at Boston Children's Hospital via CRISPR/Cas9-based zygotic mutagenesis. See Table S3 for sgRNA and genotyping information. Animals are housed at the Peking University Health Science Center Department of Laboratory Animal Science and are regularly monitored with respect to general health, cage changes, and overcrowding. Littermates of the same sex were randomly assigned to experimental groups.

To mimic the stress-induced heart injury in *Palmd* gene mutagenesis mice using isoproterenol, 8- to 12-week-old mice

were injected subcutaneously with isoproterenol ($10 \text{ mg}\cdot\text{kg}^{-1}\cdot\text{d}^{-1}$, Macklin, I822933) for 4 weeks. To study the protective role of PALMD overexpression upon isoproterenol-induced cardiac injury, isoproterenol ($50 \text{ mg}\cdot\text{kg}^{-1}\cdot\text{d}^{-1}$) was started at 4 weeks of age subcutaneously, and continued for 3 weeks.

hPSC-CM differentiation

The hESC line MEL-1 (NIHhESC-11-0139) was maintained in PGM1 hPSC culture medium (Cellapy #CA1007500, China) on plates coated with PSCeasy coating solution (Cellapy #CA3003100, China). The cells were maintained at 37°C in humidified air with 5% CO_2 . The cells were passaged at a 1:6 ratio with 0.5 mM EDTA/PBS when 80%–100% confluency was achieved.

MEL-1 cells were differentiated into cardiomyocytes by the CardioEasy human cardiomyocyte differentiation kit (Cellapy #CA2004500, China) using an established protocol [23]. In brief, when hPSCs reached 80%–95% confluency at day 0, the medium was replaced with CardioEasy differentiation medium 1. On day 2, the medium was replaced with CardioEasy differentiation medium 2. From day 4 onward, the medium was replaced with CardioEasy complete medium every other day. On day 30, cells were purified using CardioEasy cardiomyocyte purification kit (Cellapy #CA2005100, China) using an established protocol [24]. After purification, cells were maintained in CardioEasy complete medium.

The differentiated cells were digested with CardioEasy human cardiomyocyte digestion kit (Cellapy #CA2004500, China) and seeded onto glass-bottom dishes before immunofluorescence.

Plasmid

The BioID2-HA coding sequence was acquired from Addgene (#80899) [14] and subcloned into our previously published AAV-cTNT-Actn2-GFP vector (Addgene #165034) [4] to generate the AAV-cTNT-Actn2-BioID2-HA vector. Coding sequences for *Rpl7* (MMM1012-202805808) were from Dharmacon, USA. *Vcp* (MR210760), *Dpysl3* (MR220351), *Pebp1* (MR201759) and *Rack1* (MR204575) cDNA clones were purchased from Origene, USA. *Palmd*, *Pcbp1*, and *Nexn* were cloned from heart cDNA. They were subcloned into the AAV-cTNT-Actn2-GFP vector to generate GFP-tagged gene overexpression vectors.

We incorporated a miR122TS sequence into our original CASAAV vector (Addgene # #87682) [25] to generate the AAV-U6-sgRNA1-U6-sgRNA2-cTNT-Cre-miR122TS vector. This new design could reduce leaky gene editing in the liver and greatly enhanced the cardiac specificity of in vivo genome editing [26]. Next, we designed sgRNAs targeting *Palmd* using CRISPick (portals.broadinstitute.org/gppx/crispick/public) and constructed CASAAV plasmids as previously described. See Table S3 for sgRNA information.

For co-immunoprecipitation experiments, the *Palmd* and *Actn2* coding sequence was subcloned into our previously published pHA-ACTC1-R64D plasmid to generate the pHA-Palmd and pHA-Actn2 plasmid. The *Nexn* and *Actn2* coding sequence was PCR amplified from the cDNA of murine hearts and subcloned into pFLAG-MRTFA (Addgene #11978) to create the pFLAG-Nexn and pFLAG-Actn2 plasmid. The *Nexn* coding sequence was subcloned into pGFP-LA (Addgene #206197) to create the pGFP-Nexn plasmid.

AAV production and injection

AAV9 was prepared as previously described [25]. AAV titer was quantified by real-time quantitative PCR. See Table S3 for primer information. Alternatively, AAV9 was packaged at PackGene Biotech. AAV was injected into P1 pups subcutaneously, or administered into P7 pups via Intraperitoneal Injection. The pups were anesthetized in an isoflurane chamber before injection.

BioID and mass spectrometry

Animals were subcutaneously injected with AAV at P1. 24 mg/kg bodyweight biotin was intraperitoneally injected into mice twice

a day for 3 consecutive days before sample collection. 2–3 hearts were pooled in a sample. Heart tissues were homogenized with RIPA buffer containing 1% SDS with protease and phosphatase inhibitors and centrifuged at $>13,000\times g$ for 10 min to collect supernatant for BioID. Biotinylated proteins were enriched using magnetic streptavidin beads (Dyna beads M-280, Invitrogen, USA). The beads were washed with a series of SDS buffer, high salt buffer, LiCl buffer and stored in PBS at -80°C . BioID samples were validated by Simply Blue Stain (Life Technologies/Invitrogen LC6060) before mass spectrometry was performed.

Liquid chromatography with tandem mass spectrometry was performed at the Taplin Biological Mass Spectrometry Facility, Harvard Medical School, as previously described [12]. In brief, 200 ng/ μL sequencing-grade trypsin (Promega, Madison, WI) was incubated with the samples at 37°C overnight. The beads were then removed using a magnet, and the supernatant was dried in a speed-vac. The samples were re-suspended in HPLC solvent A (2.5% acetonitrile, 0.1% formic acid). A nano-scale reverse-phase HPLC capillary column was created by packing $2.6\ \mu\text{m}$ C18 spherical silica beads into a fused silica capillary (100 μm inner diameter \times $\sim 30\ \text{cm}$ length) with a flame-drawn tip. After equilibrating the column, each sample was loaded via a Famos autosampler (LC Packings, San Francisco CA). A gradient was formed, and peptides were eluted with increasing concentrations of solvent B (97.5% acetonitrile, 0.1% formic acid). As peptides eluted, they were subjected to electrospray ionization and then entered an LTQ Orbitrap Velos Elite ion-trap mass spectrometer (Thermo Fisher Scientific, Waltham, MA). Peptides were detected, isolated, and fragmented to produce a tandem mass spectrum of specific fragment ions for each peptide. Peptide sequences (and hence protein identity) were determined by matching protein databases with the acquired fragmentation pattern by the software program, Sequest (Thermo Fisher Scientific, Waltham, MA). All databases include a reversed version of all the sequences and the data were filtered to between a one and two percent peptide false discovery rate.

Echocardiography

Echocardiography was measured on mice that were anesthetized initially by 3% isoflurane and maintained asleep at 1%–1.5% isoflurane. Echocardiography was performed with a VINNO6n machine (VINNO Corporation, Suzhou, China). The standard long-axis cardiac videos were acquired using a 23 MHz transducer. FS, LVPW, and LVID values were measured by averaging results from five consecutive heart beats. The researcher who performed echocardiography was blinded to mouse genotypes.

Amplicon sequencing

Genomic DNA was extracted from tissues using TIANamp Genomic DNA Kit (DP304, Tiangen, China). The sgRNA-targeted loci of *Palmd* gene were amplified using Taq PCR MasterMix (KT211, Tiangen, China) and purified by TIANgel Purification Kit (DP219, TIANGEN). See Table S3 for primer sequences. Sequencing was performed on an Illumina NovaSeq 6000 platform at Novogene, China. The sequencing results were processed by CRISPResso2 [27].

RNA extraction and RT-qPCR

Total RNA was extracted from heart apex using the TransZol Up Plus RNA Kit (ER501-01, TransGen, Beijing, China). TransScript II One-Step gDNA Removal and cDNA Synthesis SuperMix (AH311-03, TransGen, Beijing, China) kits were used for genomic DNA removal and reverse transcription. Real-time PCR analysis was performed using Perfect Start Green qPCR Super Mix (+Dyell) (AQ602-24, TransGen, Beijing, China) and the AriaMx Real-Time PCR System (Agilent Technologies). See Table S3 for primer information.

In situ cardiac confocal imaging

Hearts were perfused with FM 4–64 (Invitrogen, 13320) on a Langendorff apparatus for 10 min at RT. The hearts were then positioned on a glass-bottom dish and immediately imaged using a Leica TCS SP8 MP FLIM inverted confocal microscope.

Cardiomyocyte isolation

Cardiomyocytes were isolated by retrograde perfusion. In brief, heparin-treated mice were anesthetized with 3% isoflurane. Hearts were extracted and cannulated onto a Langendorff perfusion apparatus. Perfusion buffer at 37°C was first pumped into the heart to flush out blood and equilibrate the heart. Collagenase II (Worthington, LS004177) was next perfused into the heart for 8 min at 37°C to dissociate cardiomyocytes. The apex was cut from the digested heart, gently dissociated into single cardiomyocytes in 10% FBS/perfusion buffer and filtered through a $100\ \mu\text{m}$ cell strainer to remove undigested tissues.

Ca^{2+} transient assay

Cardiomyocytes were isolated and reintroduced to 1.2 mM calcium. The cardiomyocytes are then incubated with $2\ \mu\text{M}$ Fura-2/AM (Yeasen, 40702ES72) at 37°C for 15 min. After three times of washes, the cardiomyocytes are resuspended and immediately analyzed using an Ion Optix Calcium and Contractility System.

Fibrosis analysis

Paraffin sectioning was performed at Servicebio, China. Heart tissues were fixed in 4% paraformaldehyde (PFA) at 4°C overnight and then in 20% sucrose solution overnight. Next, the samples were dehydrated through a serial gradient of ethanol and N-butanol. The samples were waxed in liquid paraffin for 2 h and embedded to make paraffin blocks using a tissue embedder (EG1150, Leica, Germany). Four-micron sections were cut by paraffin slicer (RM2245, Leica, Germany) and adhered to the microscope slides after floating on a water bath (HI1210, Leica, Germany).

For picrosirius red staining, the paraffin sections were dewaxed and dehydrated and then incubated with 0.2% picrosirius red solution dissolved in saturated aqueous picric acid (1.2% picric acid in water) (G1018, Servicebio). Next the sections were rinsed in water, dehydrated in increasing concentrations of ethanol, cleared in xylene and mounted for imaging using a Grundium Ocus⁴ 40 slides scanner.

TUNEL analysis

Paraffin sectioning was performed at Servicebio, China. Heart tissues were fixed in 4% PFA at 4°C overnight and then in 20% sucrose solution overnight. Next, the samples were dehydrated through a serial gradient of ethanol and N-butanol. The samples were waxed in liquid paraffin for 2 h and embedded to make paraffin blocks using a tissue embedder (EG1150, Leica, Germany). Four-micron sections were cut by paraffin slicer (RM2245, Leica, Germany) and adhered to the microscope slides after floating on a water bath (HI1210, Leica, Germany).

For TUNEL assay, the paraffin sections were deparaffinized and rehydrated and then incubated with protease K working solution (G1205, Servicebio) at 37°C to perform Antigen retrieval. Next the sections were permeabilized with permeabilised working solution (G1204, Servicebio) and equilibrium at room temperature. TUNEL reaction was performed using tunel assay kit (G1501, Servicebio; G1502, Servicebio). The sections were then counterstained with DAPI (G1012, Servicebio) and mounted for imaging using a Keyence BZ-X810 all-in-one fluorescence microscope.

Immunofluorescence analysis

Cardiomyocytes were fixed with 4% paraformaldehyde, permeabilized by 0.1% Triton-100/PBS and blocked in 4% BSA/PBS. Then

the cells were incubated with primary antibodies overnight at 4 °C and then incubated with secondary antibodies and/or dyes at RT for 2 h. The cells were mounted with ProLong Diamond antifade mountant (Invitrogen, 36961) before imaging. See Table S4 for antibody and dye information.

For immunofluorescence imaging of heart tissue, hearts were perfused with 4% paraformaldehyde on a Langendorff apparatus for 10 min at RT and then in 20% sucrose solution overnight. The samples were next embedded in OCT (Sakura) and frozen at -20 °C. Heart sections (7 µm) were cut on a cryostat microtome (CM 1950, Leica, Germany) and the following steps were the same as the cardiomyocytes.

Confocal images were taken using a Leica TCS SP8 MP FLIM laser-scanning confocal microscope with a 40×/1.5 objective. AutoTT [28] was used to quantify T-tubule, JPH2 and NEXN. Cell size and shape were manually measured using ImageJ.

Western blot analysis

Heart tissues were homogenized in RIPA buffer (25 mM Tris pH7.4, 150 mM NaCl, 1% Triton X-100, 0.5% Na Deoxycholate, 0.1% SDS) supplemented with protease inhibitor cocktail. Heart lysates were denatured in 2× SDS sample buffer at 70 °C for 10 min, separated on a 10% Bis-Tris gradient gel (Sangon Biotech, C691101-0001), transferred to a PVDF membrane, and blocked by 4% milk/TBST. Primary antibodies were incubated with the membrane overnight at 4 °C. HRP-conjugated secondary antibodies were probed for 1–2 h at RT. Chemiluminescence was detected using an Invitrogen iBright™ CL1500. See Table S4 for antibody and dye information.

Transmission electron microscopy

TEM experiments were performed by the Electron Microscopy Analysis Laboratory in the Medical and Health Analysis Center, Peking University Health Science Center. Briefly, heart samples were collected, cut into small pieces (1–2 mm cubes), and fixed in EM Grade 2.5% Glutaraldehyde (P1126, Solarbio) overnight at 4 °C. Ultrathin sections were cut using an ultramicrotome (EM UC7, Leica, Germany) and stained with uranyl acetate/lead citrate. TEM images were obtained using a transmission electron microscope (JEM-1400PLUS, Leica, Germany). All the quantifications were done using ImageJ software.

Co-immunoprecipitation assay

In vitro co-immunoprecipitation assay was performed using HEK293T cells. Cell lysates were harvested after 48 h of transfection, and were rotated overnight at 4 °C in 200 µL of IP lysis buffer (P0013, Beyotime) with 25 µL of Anti-HA/FLAG Magnetic Beads (P2121/P2132, Beyotime). After washing three times with IP lysis buffer, and two times with 1×TBS buffer (ST661, Beyotime), beads were incubated in 2× sample buffer (P1016, Solarbio) for 10 min at 70 °C. The immunoprecipitates and input lysate were then gel electrophoresed and immunoblotted.

For co-immunoprecipitation assay in heart tissues, *Palmd*^{+/+} and *Palmd*^{-/-} mice (8 weeks) hearts were harvested in IP lysis buffer and rotated overnight at 4 °C. The lysates were immunoprecipitated with protein A + G magnetic beads (P2108, Beyotime) and antibodies indicated in the paper. Rabbit non-specific IgG (A7016, Beyotime) was used as negative control. After washing three times with IP lysis buffer, and 2 times with 1×TBS buffer, beads were incubated in 2× sample buffer for 10 min at 70 °C and then gel electrophoresed and immunoblotted.

Quantification and statistical analysis

Statistics were performed using Prism (GraphPad) software. Imaging experiments were analyzed using ImageJ software. Data are presented as mean ± SD. Statistical analysis of all data was determined using the Student's *t*-test for two-group comparisons and one-way ANOVA for comparison of multiple groups. Statistical significance was defined by **P* < 0.05, ***P* < 0.01, ****P* < 0.001.

RESULTS

In vivo proximity proteomics depicts a protein atlas of Z-discs in the heart

We constructed an AAV vector to express ACTN2-BioID2 fusion protein via a cardiomyocyte-specific *Tnnt2* promoter [23]. We subcutaneously administered 5×10^{10} AAV to postnatal day 1 (P1) mice and intraperitoneally injected 24 mg/kg biotin twice a day for three days before cardiac ventricles were collected for further analysis at P14 (Fig. 1a). Western blotting showed that the AAV vector expressed ACTN2-BioID2 at a level that was much lower than endogenous ACTN2 in the heart (Fig. 1b), so the ectopic expression with BioID2 tagging was unlikely to perturb endogenous ACTN2 function or result in aberrant ACTN2 interactions. Immunofluorescence imaging of isolated cardiomyocytes demonstrated colocalization between the HA tag of ACTN2-BioID2 and cysteine and glycine-rich protein 3 (CSRP3), a classic Z-disc marker [29] (Fig. 1c). Fluorescent streptavidin also positively stained Z-discs (Fig. 1c), indicating specific proximity labeling of Z-disc-associated proteins.

We next pulled down and purified the biotinylated proteins in cardiac extracts using streptavidin beads. Coomassie blue staining and streptavidin blots demonstrated that ACTN2-BioID2 indeed triggered the biotinylation of Z-disc proteins that were absent in the control samples that did not receive AAV treatment (Fig. 1d). Endogenous ACTN2 and cardiac α -actin (ACTC1), which directly interact with ACTN2, were validated in the pulldown samples only when both AAV and biotin were given to the animals (Fig. 1b). Based on these validation data, the streptavidin beads were subjected to trypsin digestion followed by mass spectrometry-based protein analysis.

We compared the streptavidin pulldown proteomes between AAV-ACTN2-BioID2-treated samples and no AAV-treated control samples and identified 237 proteins that were significantly enriched in the ACTN2-BioID2 samples (Fig. 1e and Table S1). Gene ontology (GO) analysis showed Z-disc as the most enriched GO among Cellular Component (CC) gene sets (Fig. 1f). We manually curated each protein hit and found more than 20 proteins in our data that were previously reported to localize on Z-discs (Fig. 1g). Markers of TTs, costameres (special cell adhesion junctions in cardiomyocytes), and intercalated discs were also detected as expected (Fig. 1f, g), since these subcellular structures are tethered to myofibrils at Z-discs.

Next, we compared our data with published ACTN2-BioID data that were generated in hPSC-CMs [19]. We observed ~41% overlap among identified proteins between the two data sets (Fig. S1a). These shared hits were enriched with classic Z-disc markers (Fig. 1g and S1b), indicating that both approaches identify core Z-disc-associated proteins. By contrast, the unique hits in the in vivo data were associated with mitochondria while the hPSC-CM data were more enriched with proteins in cytoplasm (Fig. S1b). These differences agreed with the fact that postnatal cardiomyocytes undergo massive mitochondrial biogenesis, which are associated with myofibrils in vivo, while hPSC-CMs exhibit immature phenotypes with a relatively larger fractional volume of cytoplasm.

PALMD is a novel Z-disc-associated protein in mouse and human We next wondered if the ACTN2-BioID2 analysis could discover novel Z-disc-associated proteins. We manually selected seven candidate proteins in the MS data that were not yet reported to be associated with Z-discs. In part, these proteins were selected because their coding sequences fit within the limited packaging capacity of AAV, which facilitated the following validation and analysis (Fig. 2a). These candidates were selected also because their functions in the heart were poorly investigated. We constructed AAV vectors that express each candidate fused to GFP. The AAV was injected into P1 pups. At P14, we performed in situ myocardial imaging of GFP, using FM 4–64 as a marker for TTs and Z-disc [25, 30]. Among the seven candidates, palmdelphin

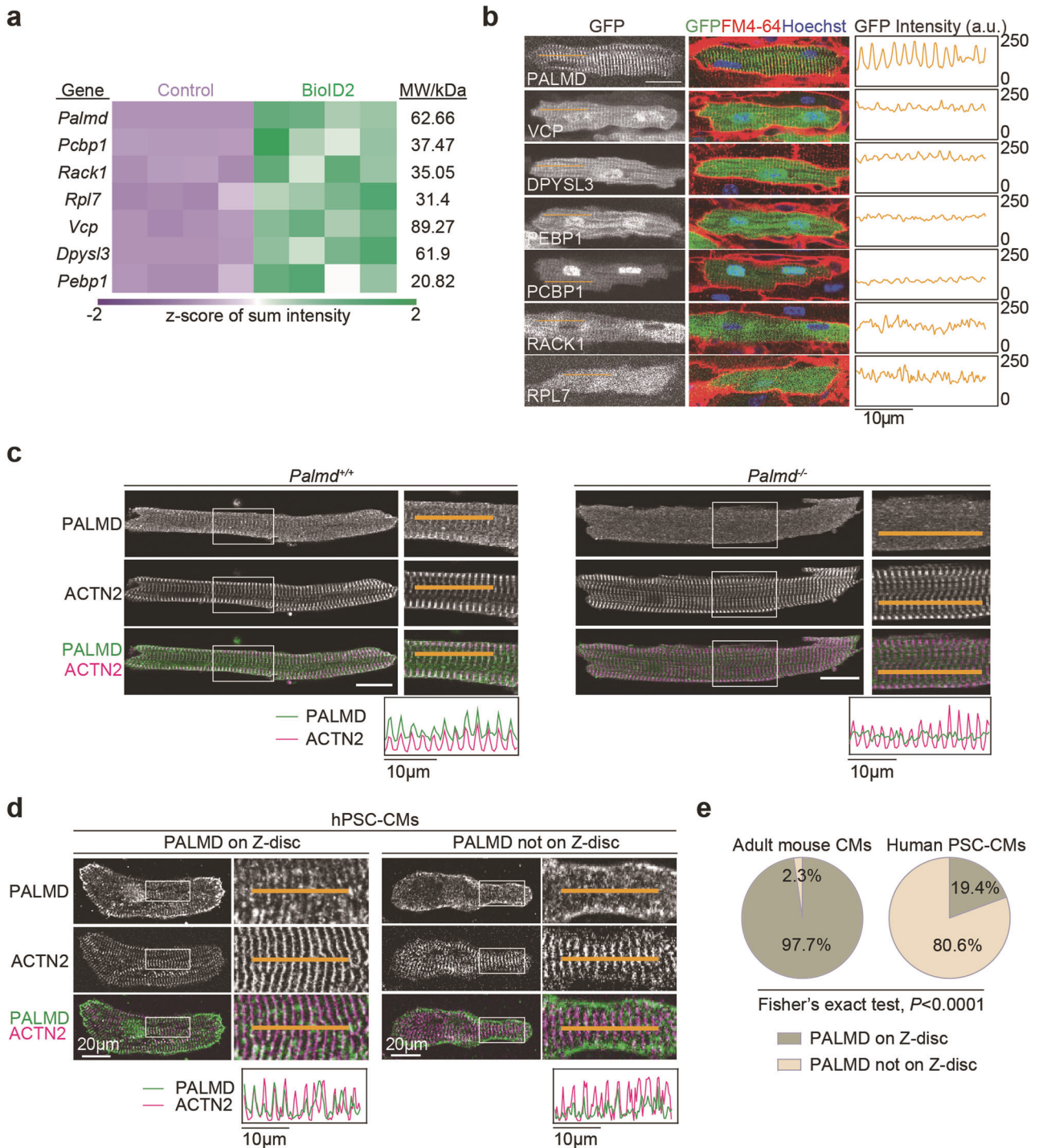


Fig. 2 In vivo proximity proteomics uncovers PALMD as a novel Z-disc-associated protein. **a** Heatmap of LC-MS/MS data for candidate proteins. MW, molecular weight. **b** In situ cardiac confocal imaging of GFP-tagged candidate proteins. The hearts were counterstained with plasma membrane/TT dye FM 4–64. Kymographs along the orange lines are shown to the right of the images. a.u., arbitrary unit. Scale bar, 20 μ m. **c** Immunofluorescence imaging of isolated adult murine cardiomyocytes. Boxed areas were enlarged to the right of the original images. The intensity of PALMD and ACTN2 signals along the orange lines are depicted in the kymographs. Scale bar, 20 μ m. **d** Immunofluorescence images of PALMD in hPSC-CMs. **e** Quantification of cell fractions with PALMD on Z-discs in adult murine cardiomyocytes ($n = 43$ cells) versus hPSC-CMs ($n = 98$ cells).

be determined. Echocardiography of adult *Palmd*^{-/-} mice demonstrated no detectable defects in systolic function or left ventricular dimensions (Fig. S3a). Immunostaining or in situ myocardial imaging analysis detected no alterations in the

organization of ACTN2 or TTs (Fig. S3b, c). Isolated cardiomyocytes also exhibited no changes of cardiomyocyte size or geometry (Fig. S3d). We previously purified murine cardiomyocytes by fluorescence-activated cell sorting and performed RNA-seq

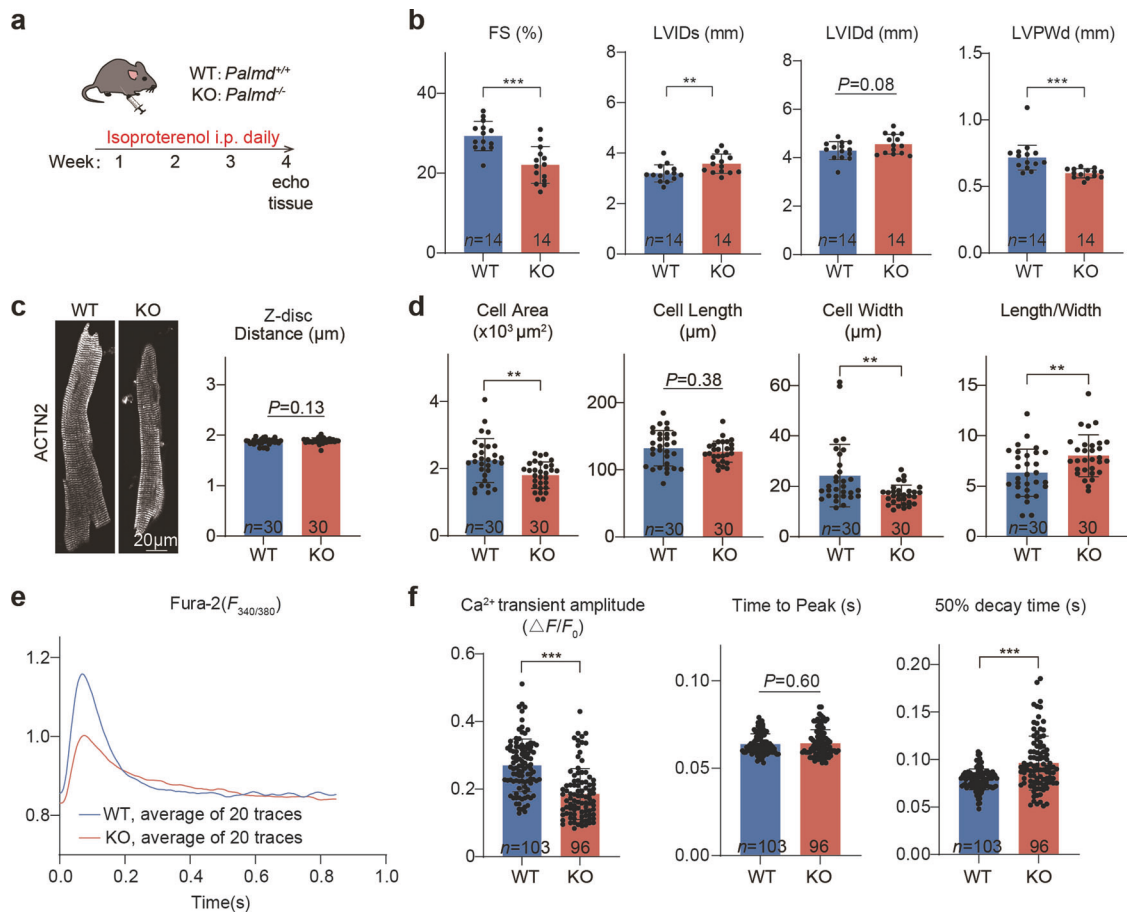


Fig. 3 *Palmd* knockout aggravates isoproterenol-induced cardiac defects. **a** Diagram of the experimental workflow. i.p., intraperitoneal injection. **b** Echocardiography of cardiac function and dimensions after 4 weeks of isoproterenol treatment. FS fractional shortening. LVIDs, end systolic left ventricular internal diameter. LVIDd, end diastolic left ventricular internal diameter. LVPWd, end diastolic left ventricular posterior wall thickness. **c** Immunofluorescence images of ACTN2 in isolated cardiomyocytes and quantification of distance between adjacent Z-discs. **d** Quantification of the size and morphology of isolated adult cardiomyocytes. **e** Average Fura-2 ratio of isolated cardiomyocytes in response to field stimulation (1 Hz). **f** Quantification of Ca^{2+} transient parameters. Student's *t* test, ** $P < 0.01$, *** $P < 0.001$, mean \pm SD. In (**b**), *n* indicates animal numbers. In (**c–f**), *n* indicates cell numbers.

analysis on serial postnatal stages during cardiomyocyte maturation [35]. This data showed that *Palmd* is the predominant paralemmin-family gene being expressed in cardiomyocytes, as compared to its homologs *Palm*, *Palm2*, and *Palm3* (Fig. S3e). Therefore, PALMD is dispensable for basal cardiomyocyte ultrastructures and functions, which cannot be explained by the redundant functions of its homologs.

We next tested whether PALMD participated in cardiac responses to stress. Isoproterenol is an adrenergic receptor agonist that is routinely applied to animals to mimic stress-induced heart injury [36]. We first administered isoproterenol daily to adult wildtype mice for 4 weeks (Fig. 3a) and then examined whether this treatment affected PALMD expression and localization. Real-time quantitative PCR (RT-qPCR) of heart tissues detected no changes in *Palmd* mRNA (Fig. S4a). Immunofluorescence and Western blot analysis identified no changes in PALMD protein levels or subcellular localization (Fig. S4b, c).

Next, we applied isoproterenol treatment to *Palmd*^{-/-} mice and performed echocardiogram (Fig. 3a). Fractional shortening (FS) appeared more impaired in *Palmd*^{-/-} mice compared to wildtype controls (Fig. 3b). Diastolic left ventricular inner diameter (LVIDd) was unaltered. Left ventricular posterior wall thickness (LVPWd) was less increased in *Palmd*^{-/-} mice (Fig. 3b). On heart sections, picrosirius red staining indicated more severe cardiac fibrosis in *Palmd*^{-/-} hearts after isoproterenol treatment

(Fig. S4d). Terminal deoxynucleotidyl transferase dUTP nick end labeling (TUNEL) demonstrated increased cell death in mutant hearts (Fig. S4e).

In isolated cardiomyocytes, ACTN2 staining detected no changes of Z-disc organization and distances (Fig. 3c). Projected cell area in mutant cardiomyocytes was less enlarged than control cells (Fig. 3d). Isoproterenol was known to induce concentric cardiac hypertrophy, which was characterized by cardiomyocyte widening and reduced length/width ratio [37]. However, in *Palmd*^{-/-} hearts, such cellular remodeling process was compromised (Fig. 3d). Together, these data showed that PALMD depletion perturbed isoproterenol-induced cardiac hypertrophy and aggravate isoproterenol-induced cardiac injury.

Z-discs serve as the scaffold for TT and SR, which mediate calcium-induced calcium release and are essential for excitation-contraction (E-C) coupling [5, 6]. Isoproterenol treatment is a well-established insult that increases the likelihood of calcium handling defects [38]. Therefore, we next measured Ca^{2+} transient in isolated Fura-2-loaded cardiomyocytes to determine if PALMD regulates calcium handling. Interestingly, we found *Palmd*^{-/-} cardiomyocytes exhibited reduced Ca^{2+} peak amplitude during cardiomyocyte contraction (Fig. 3e, f). While the time to peak showed no significant change, the 50% decay time was largely delayed, indicating defective Ca^{2+} replenishment (Fig. 3e, f).

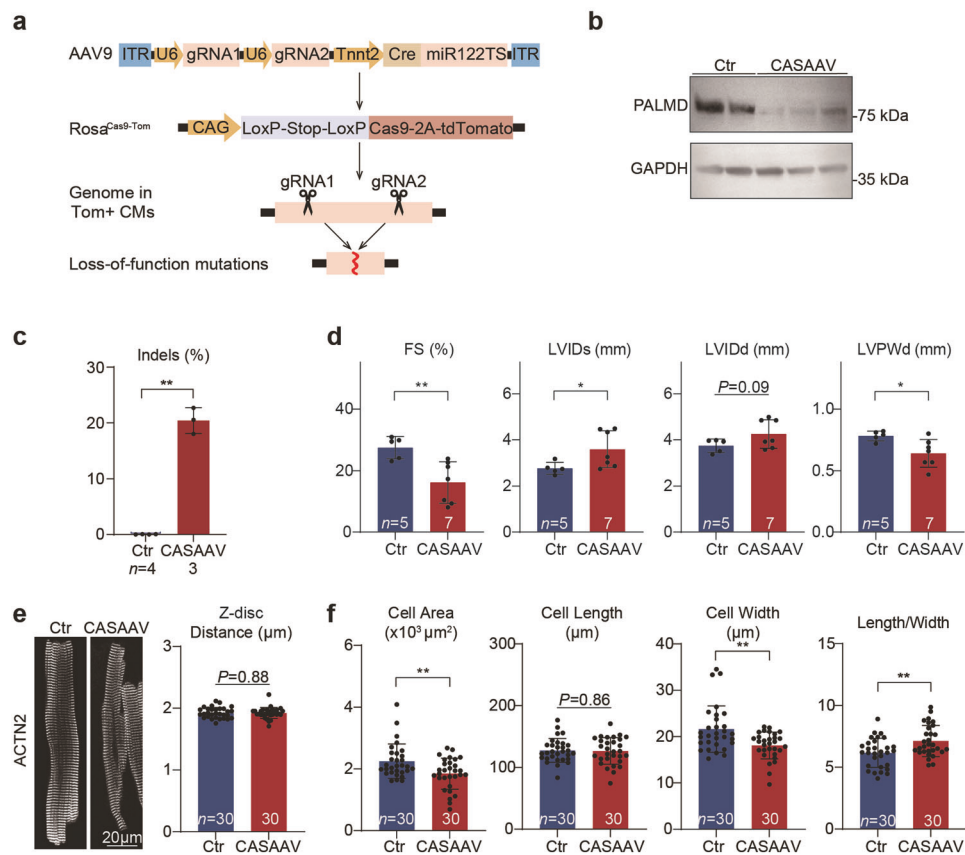


Fig. 4 CASAAB-based cardiomyocyte-specific PALMD depletion. **a** A diagram showing the workflow of CASAAB. **b** Western blot analysis of CASAAB-treated cardiac tissues. **c** Amplicon-sequencing analysis of CASAAB-targeted genome in the heart. Indel, small insertions or deletions. **d** Echocardiogram analysis of CASAAB-treated hearts. **e** ACTN2 staining on isolated cardiomyocytes and Z-disc distance quantification. **f** Size and geometry analysis of isolated cardiomyocytes. Student's *t* test, **P* < 0.05, ***P* < 0.01, mean ± SD. In (**c**, **d**), *n* indicates animal numbers. In (**e**, **f**), *n* indicates cell numbers.

Cardiomyocyte-specific PALMD depletion aggravates isoproterenol-induced cardiac injury

Because PALMD is expressed in both cardiomyocytes and non-cardiomyocytes in the heart [31], we next tested if cardiomyocyte-specific PALMD depletion is sufficient to modify isoproterenol-triggered cardiac injury. We designed two sgRNAs targeting *Palmd* and constructed AAV9 vectors expressing sgRNA along with a Cre transgene controlled by a *Tnnt2* promoter and a miR122 target sequence (miR122TS)-containing 3' untranslated region (3'UTR) [26, 39]. This vector expresses Cre specifically in cardiomyocytes and enables cardiomyocyte-specific *Palmd* somatic mutagenesis upon systemic AAV administration to Rosa^{Cas9-tdTomato} mice, which express Cas9 following Cre recombination [22, 25] (Fig. 4a).

We first validated this Cas9/AAV9-based somatic mutagenesis (CASAAB) and observed robust cardiac *Palmd* gene mutagenesis and protein depletion by amplicon-sequencing and Western blot, respectively (Fig. 4b, c, Fig. S5a, b). After isoproterenol treatment, CASAAB-treated mice exhibited more severe systolic dysfunction and compromised cardiac hypertrophy as compared to AAV-Cre treated controls (Fig. 4d). CASAAB-treated hearts also demonstrated increased interstitial fibrosis and cell death (Fig. S5c, d). Isolated cardiomyocytes exhibited size and morphology changes similar to the phenotypes in *Palmd*^{-/-} mice (Fig. 4e, f). No ACTN2 pattern or Z-disc distance phenotypes were observed (Fig. 4e, f). Thus, loss of PALMD in cardiomyocytes is sufficient to sensitize the heart to isoproterenol-induced injury and cardiac dysfunction.

PALMD overexpression mitigates isoproterenol-induced cardiac injury

Next, we asked whether PALMD overexpression was sufficient to mitigate isoproterenol-induced cardiac injury. We harnessed the AAV-GFP-Palmd vector that was also used to validate PALMD Z-disc localization (Fig. 2b) to overexpress PALMD using an AAV-GFP vector as control (Fig. 5a). Western blot analysis validated the overexpression of PALMD (Fig. 5b). Echocardiogram showed that PALMD overexpression moderately alleviated isoproterenol-induced systolic dysfunction (Fig. 5c). The PALMD overexpression also resulted in reduced cardiac fibrosis (Fig. S6a) and TUNEL-positive cell nuclei (Fig. S6b). While PALMD overexpression did not affect Z-disc organization and spacing (Fig. S6c), it triggered more pronounced cardiomyocyte enlargement, mainly due to cellular widening and reduced length/width ratio (Fig. 5d). Together, these data implied that AAV-based PALMD overexpression reduced isoproterenol-induced cardiac injury.

PALMD stabilizes NEXN on Z-disc and regulates JMCs

We next explored the potential mechanism by which PALMD modulated cardiac pathogenesis. Since PALMD depletion resulted in systolic dysfunction upon isoproterenol treatment, we first tested an array of known Z-disc-associated proteins that were required to maintain systolic function. We examined the Z-disc localization of CSR3, LIM domain binding 3 (LDB3), palladin (PALLD), myopalladin (MYPN), filamin C (FLNC), and nexilin (NEXN) in isoproterenol-treated *Palmd*^{-/-} cardiomyocytes, and observed the diminished Z-disc pattern of NEXN upon PALMD depletion

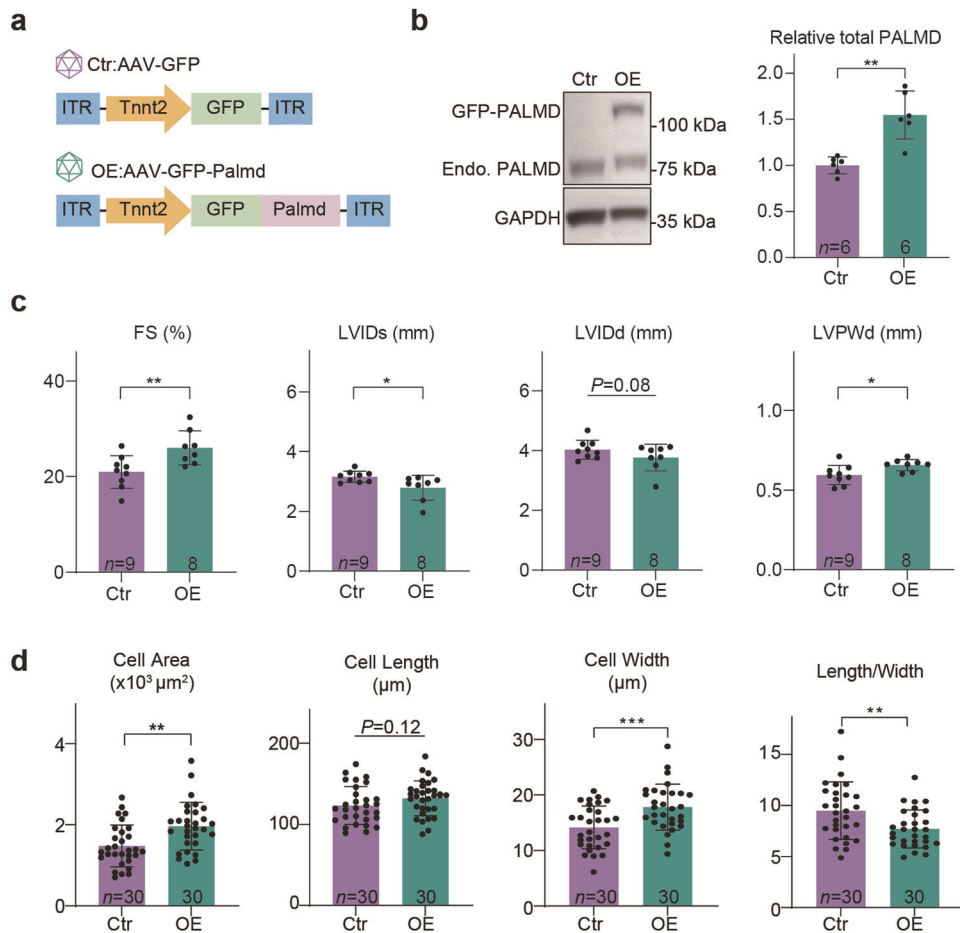


Fig. 5 PALMD overexpression alleviates isoproterenol-induced defects. **a** Diagram of the experimental workflow. Ctr, control. OE, overexpression. **b** Western blot analysis and quantification of PALMD overexpression. **c** Echocardiography of cardiac function and structure. **d** Quantification of the size and morphology of isolated adult cardiomyocytes. Student's *t* test, **P* < 0.05, ***P* < 0.01, ****P* < 0.001, mean ± SD. In (**b**, **c**), *n* indicates animal numbers. In (**d**), *n* indicates cell numbers.

(Fig. 6a and S7A). AutoTT is a software that could capture the striated patterns of Z-disc/TT-associated proteins in immunofluorescence images and quantify the patterned signals normalized to cell size [28]. We used AutoTT to measure the NEXN patterns in cardiomyocytes and further confirmed the loss of NEXN signals in the isoproterenol-treated *Palmd*^{-/-} cardiomyocytes (Fig. 6a).

Western blot analysis demonstrated significantly reduced NEXN protein levels in the isoproterenol-treated *Palmd*^{-/-} hearts (Fig. 6b) while the *Nexn* mRNA level was not influenced (Fig. S7b). As an inroad to dissect the underlying mechanism, a co-immunoprecipitation assay was performed in HEK293T cells, which showed that HA-PALMD and FLAG-NEXN could mutually pull down each other via the protein tags (Fig. 6c). Immunoprecipitation using an antibody against PALMD in heart lysates also pulled down endogenous NEXN specifically in the *Palmd*^{+/+} hearts but not the *Palmd*^{-/-} hearts (Fig. S7c). Thus, NEXN and PALMD are binding partners in the heart.

A co-immunoprecipitation assay detected the interaction between ACTN2 and NEXN (Fig. S7d), suggesting that NEXN could serve as an adaptor connecting ACTN2 to PALMD. To test this idea, the ACTN2-PALMD interaction assay (Fig S2f) was performed again in the absence or presence of NEXN. Interestingly, while PALMD failed to directly pull down ACTN2 as expected, the additional expression of NEXN resulted in clearly enhanced co-precipitation between PALMD and ACTN2 (Fig. S7e). Therefore, NEXN could serve as a linker connecting ACTN2 with PALMD.

Next, we wondered if PALMD influenced the protein stability of NEXN. Plasmids expressing PALMD and NEXN were co-transfected into HEK293T cells. Then the cells were treated with 20 μg/ml cycloheximide to block protein synthesis. As compared to cells expressing NEXN alone, we observed less decrease of NEXN in the presence of PALMD (Fig. 6d), indicating a critical role of PALMD in stabilizing NEXN protein and maintaining its protein level.

NEXN was recently shown to interact with components in JMCs and regulate TT organization [8]. In published data using proximity-labeling approaches to identify JMC or Z-disc components, PALMD and NEXN were often simultaneously detected (Table S2). These data prompted us to examine the role of PALMD in JMC and TT organization after isoproterenol treatment. In PALMD-depleted cardiomyocytes, AutoTT uncovered significantly reduced Z-disc patterns of junctophilin-2 (JPH2) [40], a structural protein that tethers TT and SR membranes at JMCs (Fig. 6e). A similar phenotype was also detected for another TT marker caveolin-3 (CAV3) (Fig. S7f). No changes of JPH2 or CAV3 protein levels were detected by Western blot (Fig. S7g), thus the reduced patterns of JPH2 and CAV3 were likely secondary to ultrastructural changes. To evaluate the ultrastructure with greater resolution, we analyzed cardiomyocytes by transmission electron microscopy. We found PALMD depletion resulted in reduced TT circularity, increased TT luminal area and increased TT distances to Z-disc (Fig. 6f). Together, these data showed that PALMD plays a crucial role in

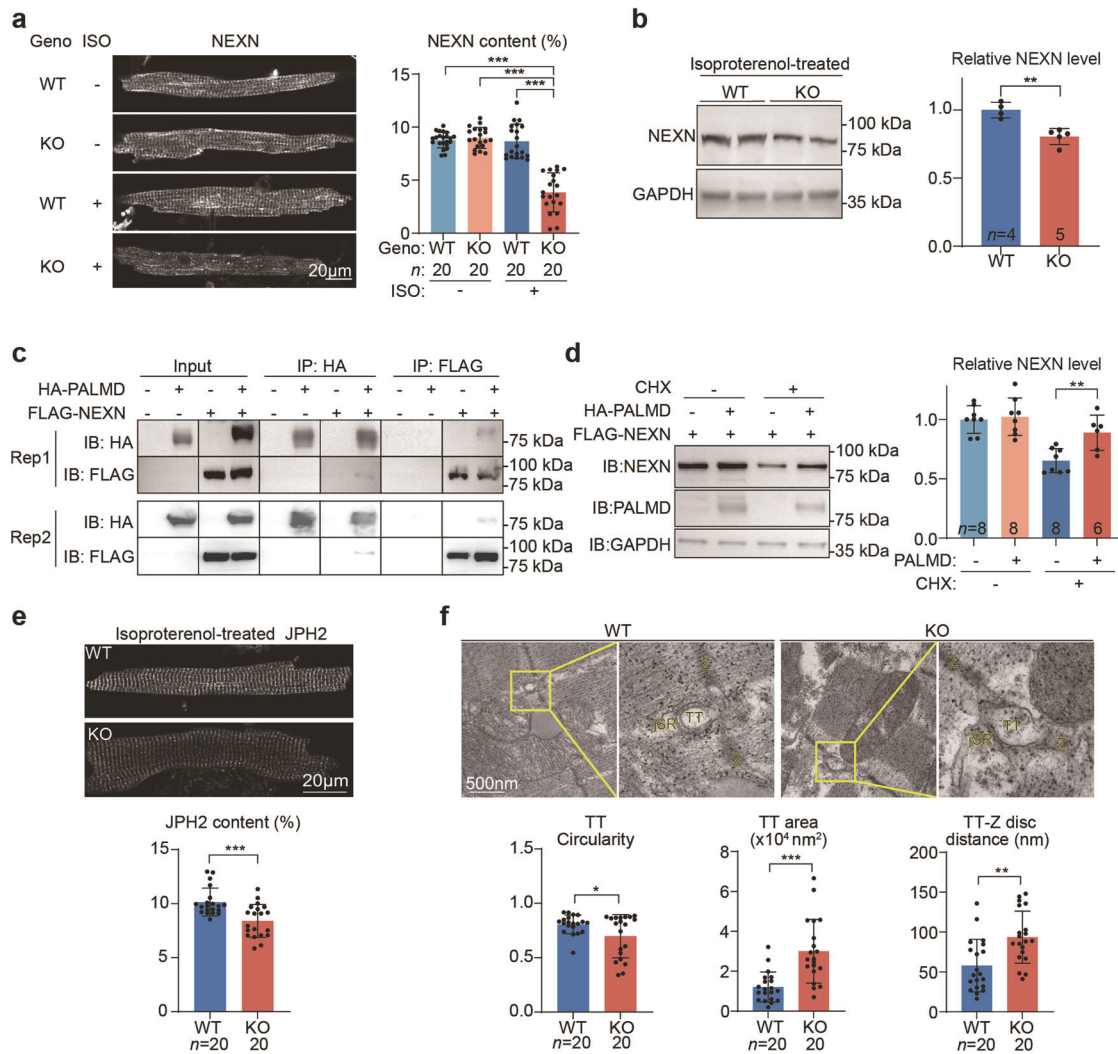


Fig. 6 PALMD modulates JMCs by stabilizing NEXN. **a** Immunofluorescence imaging and AutoTT quantification of NEXN patterns on Z-disc. ISO, isoproterenol. **b** Western blots and quantification of NEXN protein in isoproterenol-treated hearts. **c** Co-immunoprecipitation analysis between HA-PALMD and FLAG-NEXN in HEK293T cells. IP, immunoprecipitation. IB, immunoblotting. **d** Western blot analysis and quantification of NEXN in cells treated with 20 μg/ml cycloheximide for 12 h. **e** Immunofluorescence imaging and AutoTT quantification of JPH2 patterns on Z-disc. **f** Transmission electron microscopy analysis of junctional membrane complexes and quantification. TT, transverse tubule. jSR, junctional sarcoplasmic reticulum. Z z-disc. Student's *t* test, **P* < 0.05, ***P* < 0.01, *****P* < 0.001. In (**a**, **e**), *n* indicates cell numbers. In (**b**), *n* indicates animal number. In (**d**), *n* indicates repeated experiments. In (**f**), *n* indicates JMC number. Mean ± SD.

maintaining JMC/TT morphology and their association with Z-disc in the isoproterenol-stressed condition.

NEXN addback alleviates isoproterenol-induced cardiac injury in *Palmd*^{-/-} hearts

Although the above results indicated the stabilization effect of PALMD on NEXN, whether the decrease of NEXN caused the exacerbated cardiac injury in the *Palmd*^{-/-} mice after isoproterenol treatment remained unclear. To answer this question, we constructed an AAV vector to specifically express NEXN-GFP in the heart. The Z-disc/TT localization of AAV-delivered exogenous NEXN was validated by in situ confocal imaging of GFP and FM 4-64 (Fig. 7a). The AAV dosage was carefully titrated in the isoproterenol-treated *Palmd*^{-/-} hearts to restore the total NEXN level back to normal (Fig. 7b). The Z-disc pattern of NEXN was also restored in the isoproterenol-treated *Palmd*^{-/-} cardiomyocytes after AAV-Nexn treatment (Fig. 7c).

Echocardiogram validated that AAV-Nexn treatment mitigated isoproterenol-induced systolic dysfunction (Fig. 7d). The NEXN

supplementation also reduced cardiac fibrosis (Fig. S8a) and TUNEL-positive cell nuclei (Fig. S8b) in the heart. AAV-Nexn treatment did not affect the Z-disc structure (Fig. S8c), but it alleviated the cardiomyocyte hypertrophy and shape phenotypes in the *Palmd*^{-/-} mice upon isoproterenol insults (Fig. 7e). Transmission electron microscopy analysis further confirmed the restoration of the JMC/TT ultrastructural abnormality (Fig. 7f, g). Together, these data showed that NEXN reduction is indeed the key factor that causes the excessive cardiac injury in the isoproterenol-treated *Palmd*^{-/-} hearts.

DISCUSSION

Z-discs are core ultrastructural organizers of cardiomyocytes that modulate many facets of cardiac pathogenesis. Comprehensive characterization of Z-disc proteins is pivotal in the efforts to dissect molecular mechanisms and identify potential therapeutic targets for heart diseases. ACTN2-based proximity proteomics was recently reported in hPSC-CMs [19]. However, because hPSC-CMs

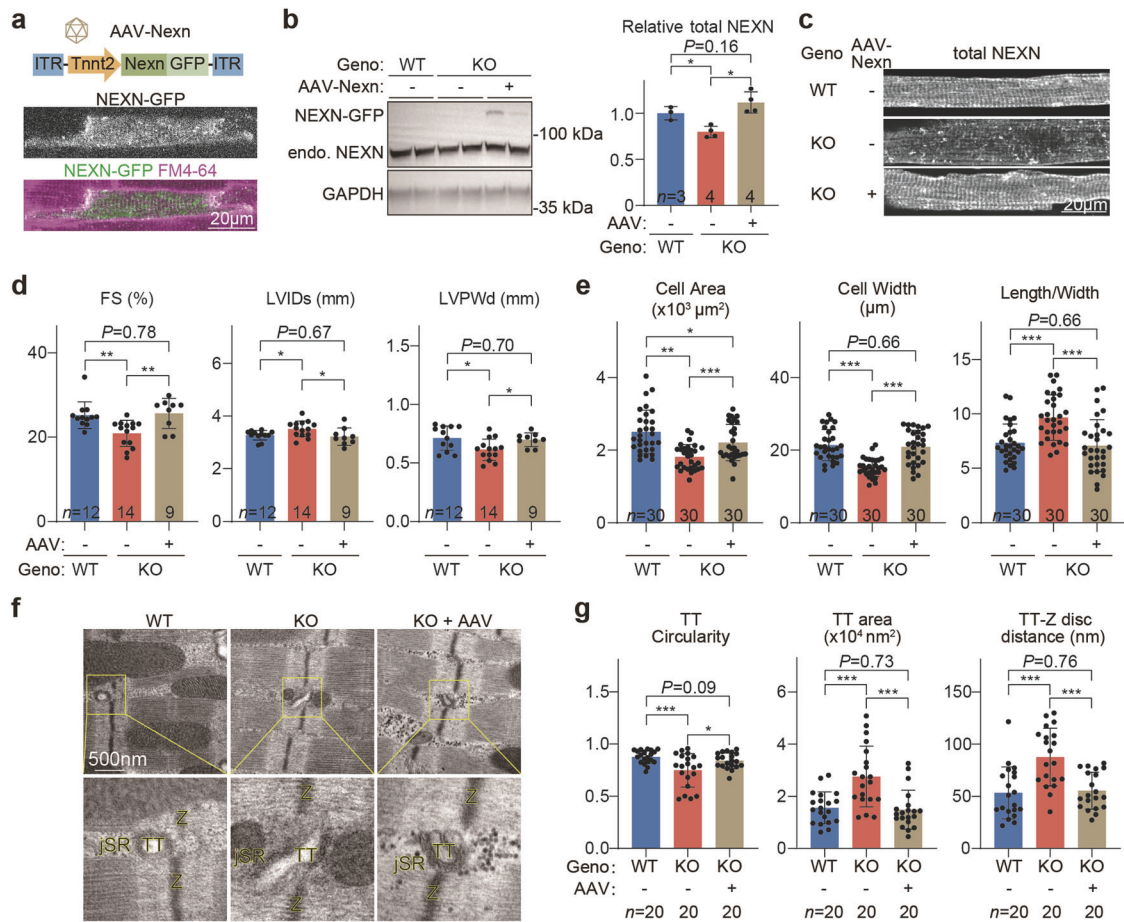


Fig. 7 NEXN addback mitigates isoproterenol-induced injury in PALMD-depleted hearts. **a** Diagram of the AAV-Nexn vector design and in situ myocardial imaging validation. **b** Western blot analysis and quantification of total NEXN expression. **c** Immunofluorescence imaging of NEXN patterns on Z-disc. **d** Echocardiography of cardiac function and structure. **e** Quantification of the size and morphology of isolated adult cardiomyocytes. **f, g** Transmission electron microscopy analysis of JMC/TT structures and quantification. TT transverse tubule. jSR junctional sarcoplasmic reticulum. Z z-disc. Student's *t* test, **P* < 0.05, ***P* < 0.01, ****P* < 0.001, mean ± SD. In **(b)** and **(d)**, *n* indicates animal numbers. In **(e)** and **(g)**, *n* indicates cell numbers.

in cell culture are known to be structurally immature, exhibiting disrupted Z-discs and TTs [20, 21], there are potential advantages in performing these studies in cardiomyocytes in vivo that have normal Z-disc structure and organization.

In this study, we established an AAV-delivered, cardiomyocyte-specific, proximity-labeling approach to characterize the Z-disc-associated proteome in vivo. We discovered an array of novel Z-disc-associated proteins and further investigated a new role of PALMD in cardiac pathogenesis. The Z-disc-associated localization of PALMD was confirmed in both murine cardiomyocytes and hPSC-CMs, but was undetected in the previous ACTN2 proximity proteomics data in hPSC-CMs [19], suggesting that the immature phenotypes of hPSC-CMs limited the set of Z-disc-associated proteins detected by proximity-labeling.

PALMD was reported to be expressed in multiple cell types in the heart. However, the function of PALMD in cardiomyocytes was unclear. In this study, we discovered PALMD to be dispensable for cardiac homeostasis in the unstressed heart. However, under isoproterenol stress, which models cardiac injury caused by chronic sympathetic activation in heart diseases, PALMD depletion resulted in aggravated cardiac injury and dysfunction. Over-expression of PALMD partially mitigated isoproterenol-induced cardiac injury, nominating PALMD as a potential therapeutic target for cardiac protection.

Strikingly, we found that PALMD played a role in stabilizing NEXN, a critical Z-disc-associated protein that was reported to regulate

both Z-disc stability and TT formation. Thus, PALMD participates in the crosstalk between Z-discs and TTs/JMCs mediated by NEXN. Mutations of many Z-disc components, including NEXN, are known to cause inherited cardiomyopathy. Therefore, further investigation of the mechanisms by which PALMD regulates NEXN under the stressed conditions would likely uncover novel molecular mechanisms behind NEXN-associated cardiomyopathy pathogenesis from the standpoint of Z-disc-JMC crosstalk.

It's worth noting that PALMD depletion, after repeated isoproterenol treatment, also perturbed other Z-disc proteins including CSRFP3, PALLD and FLNC in Fig S7a. Thus, PALMD could potentially regulate cardiomyocytes via proteins other than NEXN. Alternatively, the PALMD-NEXN complex could probably regulate other aspects of Z-disc ultrastructure in addition to TT/JMC. Further investigations are necessary to test these molecular mechanisms.

PALMD is a member of the paralemmin protein family including 4 isoforms (PALM, PALM2, PALM3 and PALMD), but the minimal baseline cardiac phenotypes are unlikely due to gene redundancy. On one hand, RNA-Seq data indicated that Palmd was expressed at a much higher level than the other three homologs (Fig. S3e). On the other hand, these genes were reported to exert distinct cellular functions due to their different biochemical properties. For example, PALM is known as a lipid raft-associated protein implicated in plasma membrane dynamics and cell shape control [41], thanks to its C-terminus prenylation and palmitoylation

modifications [42]. By contrast, the C terminus of PALMD lacks the prenyl-palmitoyl modification, thus PALMD acts more like a cytoplasmic or cytoskeletal regulator [42, 43].

The disassembly of Z-discs is a hallmark of cardiomyocyte dedifferentiation and has been observed in cardiomyocyte regeneration as well as many forms of heart diseases [44]. The AAV-ACTN2-BioID2 approach may offer a new inroad toward the dissection of cardiomyocyte dedifferentiation and cardiac pathogenesis. Future investigation of the PALMD-NEXN axis in other forms of heart diseases and in cardiac regeneration would be intriguing. Manipulation of PALMD-NEXN might also improve the maturation of hPSC-CMs, which was currently a major bottleneck in hPSC-CM applications for heart diseases [21]. In addition, further mining of the ACTN2 proximity proteomics data and investigation on other new Z-disc proteins identified in this study will likely yield new insights into cardiac pathophysiology.

CONCLUSIONS

Together, this study showed that an AAV-delivered, cardiomyocyte-specific, *in vivo* proximity proteomics approach could be harnessed to identify novel therapeutic targets for heart diseases. As an example, PALMD was discovered as a novel Z-disc-associated protein that could potentially be harnessed to mitigate isoproterenol-induced cardiac dysfunction. PALMD participated in the Z-disc-JMC/TT crosstalk and the maintenance of proper calcium handling by stabilizing NEXN.

ACKNOWLEDGEMENTS

We appreciate Taplin Mass Spectrometry Facility at Harvard Medical School for mass spectrometry analysis, Mouse Gene Manipulation Core at Boston Children's Hospital for the generation of *Palmd*^{-/-} mice, and PackGene Biotech for AAV packaging.

AUTHOR CONTRIBUTIONS

WTP and YXG provided the overall supervision; YXG conceived the research; CTG performed major experiments and analysis of PALMD subcellular localization and function in the heart; BDJ and RLA conducted BioID experiments; JSL performed echocardiogram analysis; LZJ upgraded the CASA AV vectors and managed the Rosa^{Cas9-Tom} mice; FJL provided critical guidance on the BioID protocol; QM and NM managed mouse husbandry and experiments; YPC and KLL assisted in biochemistry experiments and data analysis; CZL provided critical guidance on NEXN analysis; ZW, XJL, and FL conducted hPSC-CM analysis; MMZ, HX and EDD offered help in isoproterenol treatment experiments; YXG and CTG wrote the manuscript; WTP edited the manuscript.

FUNDING

YXG was funded by the National Key R&D Program of China (2022YFA1104800), the National Natural Science Foundation of China (82222006), the Beijing Nova Program (20220484205) and Beijing Natural Science Foundation (7232094). WTP was supported by National Institute of Health (R01HL146634 and R01HL163937). EDD was supported by the National Science Foundation of China (82070235 and 92168113), the CAMS Innovation Fund for Medical Sciences (2021-I2M-5-003) and Haihe Laboratory of Cell Ecosystem Innovation Fund (HH22KYZX0047). CZL was supported by the National Natural Science Foundation of China (82170231) and Guangdong Basic and Applied Basic Research Foundation (2023B1515020103).

ADDITIONAL INFORMATION

Supplementary information The online version contains supplementary material available at <https://doi.org/10.1038/s41401-024-01348-y>.

Competing interests: Patents have been filed relating to the data presented.

REFERENCES

1. Sanger JM, Sanger JW. The dynamic Z bands of striated muscle cells. *Sci Signal*. 2008;1:pe37.

- Lange S, Ehler E, Gautel M. From A to Z and back? Multicompartment proteins in the sarcomere. *Trends Cell Biol*. 2006;16:11–8.
- Frank D, Frey N. Cardiac Z-disc Signaling Network. *J Biol Chem*. 2011;286:9897–904.
- Guo YX, Cao YP, Jardin BD, Sethi I, Ma Q, Moghadaszadeh B, et al. Sarcomeres regulate murine cardiomyocyte maturation through MRTF-SRF signaling. *Proc Natl Acad Sci USA*. 2021;118:e2008861118.
- London B. Defining the complexity of the junctional membrane complex. *Circ Res*. 2017;120:11–2.
- Hong TT, Shaw RM. Cardiac T-tubule microanatomy and function. *Physiol Rev*. 2017;97:227–52.
- Hassel D, Dahme T, Erdmann J, Meder B, Hugel A, Stoll M, et al. Nexilin mutations destabilize cardiac Z-discs and lead to dilated cardiomyopathy. *Nat Med*. 2009;15:1281–U78.
- Liu CZ, Spinozzi S, Chen ZY, Fang X, Feng W, Perkins G, et al. Nexilin is a new component of junctional membrane complexes required for cardiac T-tubule formation. *Circulation*. 2019;140:55–66.
- Wang H, Li Z, Wang J, Sun K, Cui Q, Song L, et al. Mutations in NEXN, a Z-disc gene, are associated with hypertrophic cardiomyopathy. *Am J Hum Genet*. 2010;87:687–93.
- Kushner JS, Liu GX, Eisert RJ, Bradshaw GA, Pitt GS, Hinson JT, et al. Detecting cardiovascular protein-protein interactions by proximity proteomics. *Circ Res*. 2022;130:273–87.
- Rees JS, Li XW, Perrett S, Lilley KS, Jackson AP. Protein neighbors and proximity proteomics. *Mol Cell Proteom*. 2015;14:2848–56.
- Lu F, Ma Q, Xie W, Liou CL, Zhang D, Sweat ME, et al. CMYA5 establishes cardiac dyad architecture and positioning. *Nat Commun*. 2022;13:2185.
- Roux KJ, Kim DI, Raida M, Burke B. A promiscuous biotin ligase fusion protein identifies proximal and interacting proteins in mammalian cells. *J Cell Biol*. 2012;196:801–10.
- Kim DI, Jensen SC, Noble KA, Birendra KC, Roux KH, Motamedchaboki K, et al. An improved smaller biotin ligase for BioID proximity labeling. *Mol Biol Cell*. 2016;27:1188–96.
- Lam SS, Martell JD, Kamer KJ, Deerinck TJ, Ellisman MH, Mootha VK, et al. Directed evolution of APEX2 for electron microscopy and proximity labeling. *Nat Methods*. 2015;12:51–4.
- Liu GX, Papa A, Katchman AV, Zakharov SI, Roybal D, Hennessey JA, et al. Mechanism of adrenergic Cav1.2 stimulation revealed by proximity proteomics. *Nature*. 2020;577:695–+.
- Feng W, Liu CZ, Spinozzi S, Wang L, Evans SM, Chen J. Identifying the cardiac dyad proteome *in vivo* by a BioID2 knock-in strategy. *Circulation*. 2020;141:940–2.
- Rudolph F, Fink C, Hüttemeier J, Kirchner M, Radke MH, Lopez Carballo J, et al. Deconstructing sarcomeric structure-function relations in titin-BioID knock-in mice. *Nat Commun*. 2020;11:3133.
- Ladha FA, Thakar K, Pettinato AM, Legere N, Ghahremani S, Cohn R, et al. Actinin BioID reveals sarcomere crosstalk with oxidative metabolism through interactions with IGF2BP2. *Cell Rep* 2021;36:109512.
- Guo YX, Pu WLT. Cardiomyocyte maturation new phase in development. *Circ Res*. 2020;126:1086–106.
- Yang XL, Pabon L, Murry CE. Engineering adolescence maturation of human pluripotent stem cell-derived cardiomyocytes. *Circ Res*. 2014;114:511–23.
- Lin J, Chen Z, Yang L, Liu L, Yue P, Sun Y, et al. Cas9/AAV9-mediated somatic mutagenesis uncovered the cell-autonomous role of sarcoplasmic/endoplasmic reticulum calcium ATPase 2 in murine cardiomyocyte maturation. *Front Cell Dev Biol*. 2022;10:864516.
- Lian XJ, Hsiao C, Wilson G, Zhu KX, Hazeltine LB, Azarin SM, et al. Robust cardiomyocyte differentiation from human pluripotent stem cells via temporal modulation of canonical Wnt signaling. *Proc Natl Acad Sci USA*. 2012;109:E1848–E57.
- Tohyama S, Fujita J, Hishiki T, Matsuura T, Hattori F, Ohno R, et al. Glutamine oxidation is indispensable for survival of human pluripotent stem cells. *Cell Metab*. 2016;23:663–74.
- Guo YX, VanDusen NJ, Zhang LN, Gu WL, Sethi I, Guatimosim S, et al. Analysis of cardiac myocyte maturation using CASA AV, a platform for rapid dissection of cardiac myocyte gene function *in vivo*. *Circ Res*. 2017;120:1874–+.
- Yang L, Liu Z, Chen G, Chen Z, Guo C, Ji X, et al. MicroRNA-122-mediated liver targeting enhances the tissue specificity of cardiac genome editing. *Circulation*. 2024;149:1778–81.
- Clement K, Rees H, Canver MC, Gehrke JM, Farouni R, Hsu JY, et al. CRISPResso2 provides accurate and rapid genome editing sequence analysis. *Nat Biotechnol*. 2019;37:224–6.
- Guo A, Song LS. AutoTT: automated detection and analysis of T-tubule architecture in cardiomyocytes. *Biophys J*. 2014;106:2729–36.
- Rashid MM, Runci A, Polletta L, Carnevale I, Morgante E, Foglio E, et al. Muscle LIM protein/CSR3: a mechanosensor with a role in autophagy. *Cell Death Discov*. 2015;1:15014.

30. Chen B, Zhang C, Guo A, Song LS. In situ single photon confocal imaging of cardiomyocyte T-tubule system from Langendorff-perfused hearts. *Front Physiol.* 2015;6:134.
31. Sáinz-Jaspeado M, Smith RO, Plunde O, Pawelzik SC, Jin Y, Nordling S, et al. Palmelphin regulates nuclear resilience to mechanical stress in the endothelium. *Circulation.* 2021;144:1629–45.
32. Wang S, Yu H, Gao J, Chen J, He P, Zhong H, et al. PALMD regulates aortic valve calcification via altered glycolysis and NF- κ B-mediated inflammation. *J Biol Chem.* 2022;298:101887.
33. Li Z, Gaudreault N, Arsenault BJ, Mathieu P, Bossé Y, Thériault S. Phenome-wide analyses establish a specific association between aortic valve PALMD expression and calcific aortic valve stenosis. *Commun Biol.* 2020;3:477.
34. Thériault S, Gaudreault N, Lamontagne M, Rosa M, Boulanger MC, Messika-Zeitoun D, et al. A transcriptome-wide association study identifies PALMD as a susceptibility gene for calcific aortic valve stenosis. *Nat Commun.* 2018;9:988.
35. Guo Y, Jardin BD, Zhou P, Sethi I, Akerberg BN, Toepfer CN, et al. Hierarchical and stage-specific regulation of murine cardiomyocyte maturation by serum response factor. *Nat Commun.* 2018;9:3837.
36. Leenen FHH, White R, Yuan BX. Isoproterenol-induced cardiac hypertrophy: role of circulatory versus cardiac renin-angiotensin system. *Am J Physiol-Heart C.* 2001;281:H2410–H6.
37. Nakamura M, Sadoshima J. Mechanisms of physiological and pathological cardiac hypertrophy. *Nat Rev Cardiol.* 2018;15:387–407.
38. Papa A, Kushner J, Marx SO. Adrenergic regulation of calcium channels in the heart. *Annu Rev Physiol.* 2022;84:285–306.
39. Yang L, Liu Z, Chen G, Chen Z, Guo C, Ji X, et al. MicroRNA-122-mediated liver detargeting enhances the tissue specificity of cardiac genome editing. *Circulation.* 2024;149:1778–81.
40. Landstrom AP, Beavers DL, Wehrens XHT. The junctophilin family of proteins: from bench to bedside. *Trends Mol Med.* 2014;20:353–62.
41. Hultqvist G, Ocampo Daza D, Larhammar D, Kilimann MW. Evolution of the vertebrate paralemmin gene family: ancient origin of gene duplicates suggests distinct functions. *PLoS One.* 2012;7:e41850.
42. Hu B, Copeland NG, Gilbert DJ, Jenkins NA, Kilimann MW. The paralemmin protein family: identification of paralemmin-2, an isoform differentially spliced to AKAP2/AKAP-KL, and of palmelphin, a more distant cytosolic relative. *Biochem Biophys Res Commun.* 2001;285:1369–76.
43. Hu B, Petrasch-Parwez E, Laue MM, Kilimann MW. Molecular characterization and immunohistochemical localization of palmelphin, a cytosolic isoform of the paralemmin protein family implicated in membrane dynamics. *Eur J Cell Biol.* 2005;84:853–66.
44. Zhu YK, Do VD, Richards AM, Foo R. What we know about cardiomyocyte dedifferentiation. *J Mol Cell Cardiol.* 2021;152:80–91.

Springer Nature or its licensor (e.g. a society or other partner) holds exclusive rights to this article under a publishing agreement with the author(s) or other rightsholder(s); author self-archiving of the accepted manuscript version of this article is solely governed by the terms of such publishing agreement and applicable law.